RESEARCH ARTICLE

WILEY

An empirical transcendental hysteresis model for structural systems with pinching and degradation

Angelo Aloisio[1] [ORCID] | **Petr Sejkot[2]** | **Asif Iqbal[3]** | **Massimo Fragiacomo[1]**

[1] Civil and Environmental Engineering Department, Università degli Studi dell'Aquila, L'Aquila, Italy

[2] Klokner Institute, Czech Technical University in Prague, Czech Republic

[3] Department of Civil Engineering, University of Northern British Columbia, Prince George, Canada

Correspondence
Angelo Aloisio PhD, Civil and Environmental Engineering Department, Università degli Studi dell'Aquila, L'Aquila, 67100, Italy.
Email: angelo.aloisio1@univaq.it

Abstract

The authors present a novel transcendental hysteresis model based on the piecewise definition of arctangent functions. The definition of the shape parameters of the arctangent functions originates from the features of the experimental hysteresis curves directly. In the first step, the authors present this model's application to the experimental cyclic response of cross-laminated timber (CLT), light-timber frame (LTF) shear walls, and a steel angle bracket. Then, the response of a plywood-coupled laminated-veneer lumber (LVL) shear wall is used for validation purposes. The paper introduces the arctangent-based model, labeled Atan model, by illustrating some possible shortcomings of hysteresis models with pinching. The paper concludes with a simple demonstration of these issues in the case of a Bouc-Wen class hysteresis model, the extended energy-dependent generalized Bouc-Wen (eegbw) model. The numerical instabilities of the eegbw model are used to endorse the advantages of the proposed formulation in modeling complex structural arrangements, like wood joints and structural systems. The proposed model originates from the analysis of the experimental response of wood joints. However, it can be of more general application, and the particular reference to wood joints does not preclude other application fields.

KEYWORDS
cross-laminated timber, hysteresis models, light-timber frame, pinching, shear walls, timber engineering

1 | INTRODUCTION

Many of the recent research efforts in structural dynamics and earthquake engineering focus on predicting the inelastic response of real structures[1] or structural archetypes.[2–4] However, the analyses of rather elementary structures may require significant computational efforts. Consequently, the nonlinear dynamic analyses of more complicated systems are not feasible unless simplified methods are adopted.[5] Among them, the use of empirical hysteresis models can significantly reduce the computational costs of nonlinear dynamic analysis.[6–9] Empirical hysteresis models aim at reproducing the experimental response of the structural system without concern on the mechanics of materials: the model is empirical, i.e., it blindly matches the experimental data.

Like timber ones, many structures descend from the assemblage of timber elements using steel connectors. The empirical modeling of each connector using empirical hysteresis formulations rather than the finite element (FE) modeling of the connector can significantly ease the numerical simulations of complicated structural arrangements. In the scientific

literature, there are a variety of empirical hysteresis models, and many models attempt to reproduce the complex phenomena of timber connections: pinching, strength degradation, and stiffness degradation.[10–12] The need to account for these phenomena entails more complex mathematical formulations, like in Ref. [13]

There are two main categories of hysteresis models in structural engineering applications: differential and nondifferential.[14] Differential models originate from Volterra's pioneering studies at the beginning of the last century. Still, the history of hysteresis (i.e., rate-independent memory) is relatively short: mathematical developments lag behind those of physicists and engineers. It was only in 1966 that hysteresis was first given a functional approach by Bouc, who introduced a differential hysteresis model,[15] later extended by Yi-Kwei Wen, Baber, and Noori.[16] The Bouc-Wen-Baber-Noori BWBN model of hysteresis is one of the most used hysteretic models to describe nonlinear hysteretic systems. This model can follow a wide range of hysteretic shapes. Foliente[17] modified the BWBN and applied the model to wood structures. Although the Bouc-Wen class models are the most used in structural engineering, the Bouc-Wen class models do not encompass all possible differential models. The mathematicians introduced the notion of hysteresis operator,[18] which aims to unify all mathematical formulations possibly valid for an ample variety of hysteresis phenomena. The scientific literature is abundant of hysteresis models striving for generality and versatility[19]; However, most of the research in structural engineering, chiefly directed on applications, does not deal with differential hysteresis models more evolved than the Bouc-Wen class ones and focalizes on nondifferential formulations due to flaws and challenges in using these models. The Bouc-Wen class model, for instance, suffers from some shortcomings and requires a consistent definition of the parameters to obtain upper bounded results.[20] Additionally, the exact modeling of pinching, characterized by a notable boost in stiffness, may cause several convergence problems.[21,22] Besides, the digital era's ascension has lessened the energies of structural engineers devoted to the study of analytical models and praised more elementary approaches based on the use of piecewise functions.

Therefore, many scholars dedicated their research to algebraic or transcendental hysteresis models, which may have some stability advantages to the differential ones: they are generally faster and less computationally demanding. Algebraic hysteresis models refer to the formulations based on polynomial expressions, while transcendental ones originate from transcendental functions. Algebraic and transcendental models are nondifferential models, compared to the well-known Bouc-Wen, which is defined as a first ordinary differential equation (ODE).

In the field of timber engineering, a few scholars presented algebraic empirical hysteresis model, and most of them descend from the piecewise definition of linear functions, like the models by Polensek and Laursen,[23] the trilinear model by Rinaldin et al.,[24] and the SAWS Material Model (OpenSees).[25] Conversely, the Consortium of Universities for Research in Earthquake Engineering (CUREE) model,[26] the evolutionary parameter hysteretic model (EPHM),[27] and others[28,29] present nonlinear branches. Dolan[30,31] developed a transcendental hysteresis model based on four exponential functions that define the hysteretic curves. Differential models are continuous since they descend from the solution of a differential equation. Algebraic or transcendental models must achieve continuity by choosing the several curves that compose the entire cycle. In contrast with the differential models, a specific concern must be given to fulfil the continuity conditions, satisfied by all the models referenced above. Additionally, an essential aspect regards the convenience of adopting hysteretic models defined by a single function rather than multilinear ones characterized by continuity conditions, as remarked by Refs. [32–35]. Compared to other engineering fields, most of the research on timber engineering still focalizes on the experimental testing of structural assemblies. The prediction of timber arrangements' inelastic response still requires a consistent validation with experimental tests, since FE analyses are time-consuming and affected by significant uncertainties. The uncertainties mainly relate to the unknown interaction between timber and the connectors and the actual force distribution inside the structure. In this paper, the authors discuss a novel transcendental hysteresis model, possibly useful for modeling wooden joints or structural systems *tout court*. The first sections qualitatively discuss the numerical issues associated with empirical hysteresis model with pinching. Then, the following sections present the model and its application to a class of structural systems. The last section addresses the issue of numerical stability by referring to a Bouc-Wen class model.

2 | STABILITY ISSUES OF HYSTERESIS MODELS WITH PINCHING

The current research stems from the solution of the numerical instabilities related to a drastic change in stiffness. The authors strived for an elementary and versatile solution based on the use of the arctangent function. Still, this function's choice is arbitrary, and its use does not guarantee a good agreement with any possible hysteresis curve. The optimum parameters of the selected function do not always ensure sufficient flexibility. The proposed method is not different from
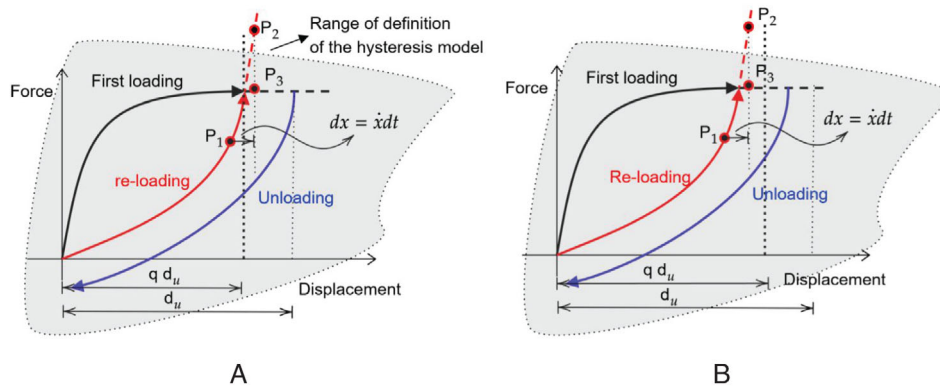
FIGURE 1 Illustration of the modeling issues behind hysteresis models with pinching; x is the displacement, $\dot{x}$ the velocity, d_u the ultimate displacement, q the pinching fraction, dt the time step

other ways of defining hysteresis loops using different functions. Besides, the solution of additional numerical issues, like the accumulation of error over multiple time-steps, is not the object of this research, which converges on a specific problem often encountered in pinched models. The following paragraphs present a qualitative introduction to the numerical instability problems recurrent in pinched models due to the drastic change in stiffness. The modeling of hysteresis phenomena characterized by pinching effects requires two definitions of the loading paths. The first loading has an initial higher stiffness while approaching an upper force bound with a lower inclination. The reloading has lower stiffness due to the occurred plasticization. However, while reloading, the stiffness boosts before attaining a fraction (q) of the maximum displacement of the first loading (d_u). The stiffness value rises rapidly, almost instantaneously, due to the occurring of pinching. After the almost abrupt growth, the curve reconnects to the first loading path, see Figure 1(A). The two curves, needed to replicate the first loading and pinched paths, have opposite curvatures. The former resembles a concave function, the latter a convex one. The former is more stable and tends to a nearly horizontal asymptote, depending on hardening phenomena. The latter boosts and has an almost vertical asymptote, even before the attaining of the ultimate displacement. Figure 1 illustrates the concept by extrapolating the curves with the dotted line. Accurate modeling demands the selection of two functions with the same curvatures as the curves to be replicated. The authors challenged in accurately modeling complex hysteresis phenomena and attempted to extend the generalized Bouc-Wen model to pinching and degradation.[13] However, they realized that the model is very stable in pseudo-static simulations, but suffers instability issues when dealing with dynamics. The instability is prevented by reducing the integration step significantly. Still, the considerable lowering of the integration step makes the simulation very time consuming. To the authors' knowledge, similar instability issues are indeed the flaw of all empirical hysteresis models with pinching. The substantive reason behind numerical instability and difficulties in numerical convergence is elementary. The authors attempted to explain in Figures 1(A) and 1(B). The points P_1, P_2, and P_3 represent three possible time-instants of a dynamic simulation. When dealing with pseudo-static simulations, prevalent in structural engineering, the velocity ($\dot{x}$) is constant and shallow. Consequently, the displacement step (dx) can be tiny, even with looser time steps (dt), being $dx = \dot{x}dt$. The time-discrete equation that describes the displacement at a certain time step is:

$$x(t_{k+1}) = x(t_k) + \dot{x}(t_k)dt, \tag{1}$$

$$\dot{x}(t_k) = \text{constant}, \tag{2}$$

where t_k is the k-th time step. Accurately, the primary reason beneath instability is the definition of the transition between the first loading and the pinched paths inside a for-loop, conventionally based on a conditional statement.

If $\{x(t_k) > q \cdot d_u \,|d_u = \max(x(t_k)) \forall t_k | k \in [0, k]\}$ Then
$x(t_k) =$ First loading
Else
$x(t_k) =$ Re-loading

If the displacement $x(t_k)$ at the time t_k, attained during the entire time history up to t_k, is higher than $q \cdot d_u$, the algorithm selects the first loading curve in the successive time step. Otherwise, the following point remains in the pinched curve. In pseudo-static simulations the displacement step can be tiny without significant extension of the computation time: the threshold $q \cdot d_u$ passes very close to the intersection point between the first-loading and the reloading curve. Hence, the conditional statement sharply defines the transition between the two functions.

Conversely, in dynamic simulations, like seismic excitation, the velocity is unknown and descends from the dynamic equilibrium equation. The time-discrete dynamic equilibrium equations of a single-degree-of-freedom (SDOF) oscillator subjected to a base seismic excitation can be written as:

$$x(t_{k+1}) = x(t_k) + \dot{x}(t_k)dt, \tag{3}$$

$$\dot{x}(t_{k+1}) = \dot{x}(t_k) - [2\xi\omega\dot{x}(t_k) - \omega^2 x(t_k) - a_g(t_k)], \tag{4}$$

where ξ is the viscous damping, ω the natural pulsation, and $a_g(t)$ the seismic base excitation. When the velocity is consistently high, the displacement step may be higher than expected, even if the time step is tiny. If so, the definition of the conditional threshold d_u is not very sharp, and may fall beyond the intersection point between the first-loading and reloading curves. Consequently, the algorithm selects point P_2 after P_1, rather than P_3. Therefore, convergence would be compromised. The point P_1 may jump to point P_2 in a single time step, directly. However, the pinched path can be so perpendicular, that the point may fall far beyond the definition of the hysteresis model, approaching infinity. When the point of integration befalls in that region, the simulation is very unlikely to converge and lacks any physical meaning, since the hysteresis model maybe not defined in that region. In conclusion, some numerical instabilities descend from the combination of two effects: (i) the velocity increases the displacement step and (ii) the significant inclination of the pinched paths. (i) The former determines the inaccurate definition of the maximum displacement reached in the previous cycles, which should be very close to the intersection point between the first-loading and reloading curves to achieve a smooth transition. (ii) The latter compromises the numerical stability since the erroneously selected point would exceed the definition of the hysteresis model.

2.1 | Enhancing numerical stability of pinched model

There are two alternatives to enhance the numerical stability of hysteresis models with pinching: (i) sharpening the definition of the shifting threshold (d_u) or (ii) selecting upper bounded functions to replicate pinched paths. (i) A refined definition of d_u requires a direct control on the amplitude of the displacement step, dx, which must remain below a specific value ($d\hat{x}$). If dx exceeds that value, the algorithm should initiate a while loop, which reduces the amplitude of the time step until the condition's fulfilment. However, implementing this additional task to an advanced model may arise some concerns about the actual advantages of using convex functions to match pinched loading curves. Additionally, the convergence of the while loop would entail an inexorable increase in the computational costs. (ii) On the contrary, selecting alternative concave functions to match pinched paths, characterized by opposite curvature, determines an overestimation of the dissipated energy in the range $[0 - q \cdot d_u]$. The sensitivity of dynamic simulations to accurate modeling of pinching is the discrimination between the two options above. Does the neglection of pinching determine biases in numerical simulations significant for engineering purposes? Besides, in possible hysteresis models defined by upper bounded functions, the extra-energy caused by concave functions may be compensated by a mindful calibration of the other modeling parameters. In this paper, the authors examine the second option by comparing two hysteresis models. First, they present the definition of alternative transcendental hysteresis models based on upper bounded trigonometric functions. The authors then challenge these models in seizing the hysteresis response of assorted experimental data, corresponding to a variety of structural systems. The last sections bestow the testing of two models, the extended energy-dependent generalized Bouc-Wen (eegbw) model and the current one. The two models match the outcomes of pseudo-dynamic experimental tests. Next, the authors discuss the results and analyze their stability by varying the integration velocity within a specific range.
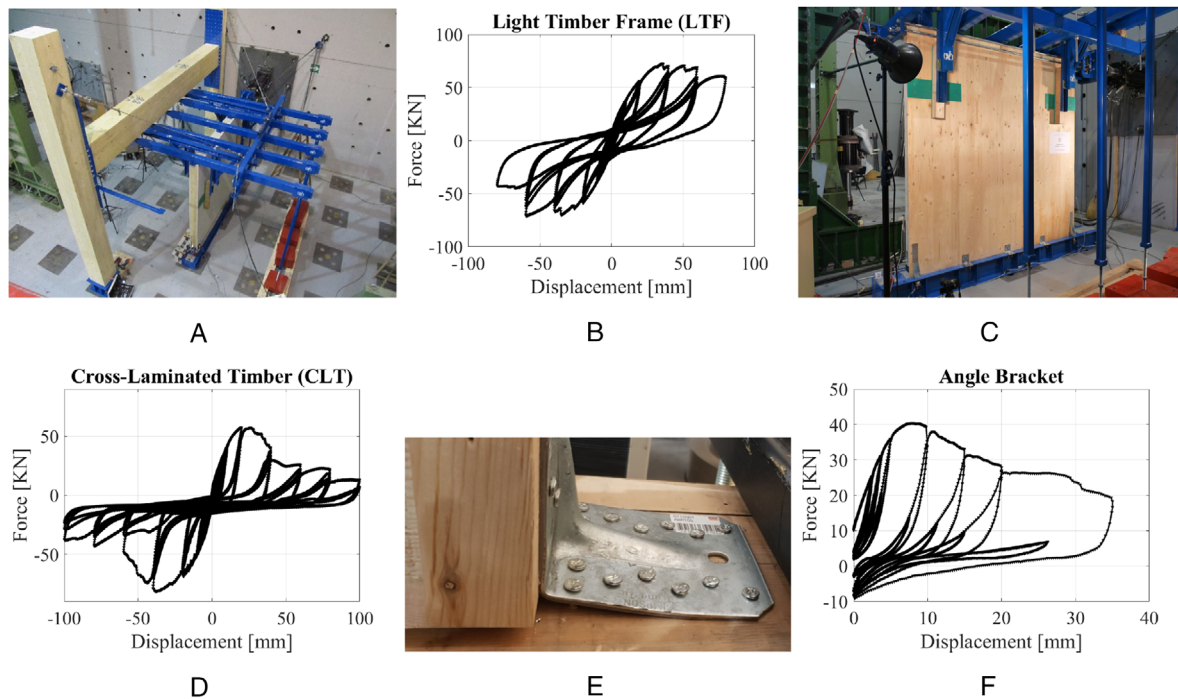
FIGURE 2 Examples of the cyclic responses of LTF (A) and (B) and CLT panels (C) and (D) carried out in the laboratories of the University in Trento, Italy. Grossi et al. provide full detail of the experimental setup in Ref. [36]. (E) and (F) Pull out tests of angle brackets carried out in the laboratories of the Northern Columbia University

3 | ALTERNATIVE MODELING OF WOOD-JOINTS AND STRUCTURAL SYSTEMS

Next to the numerical issues behind the accurate modeling of pinching using convex functions, another evidence may benefit a mindful formulation of a class of hysteresis models.

Specifically, many structural systems, like light-timber frame (LTF), cross-laminated timber (CLT), exhibit a significant stiffness reduction in the unloading phases when attaining lower displacement values after an initial force drop. Consequently, the hysteresis curves mostly evolve in the first and third quadrants of the Cartesian plane: the curves marginally traverses the second and the fourth quadrants. Figure 2 show the cyclic load tests on LTF and CLT shear walls: the curves almost intersect the axes' origin during the unloading phases. After an initial force drop, the unloading curves have a shallow slope, which allows going back to lower deformations almost without crossing the second and fourth quadrants. The scholar can adequately select the unloading functions depending on the class of hysteresis phenomena to reproduce. Precisely, he can base the ones considered in this paper, distinguished by a reduced energy dissipation due to pinching, on the use of inverse trigonometric functions, like the arctangent. Arctangent is upper bounded:

$$\arctan : \mathbb{R} \to \left(-\frac{\pi}{2}, \frac{\pi}{2} \right) \tag{5}$$

and its first derivative approaches zero very rapidly. Consequently, the arctangent meets the requirement explained at the beginning of the section: the unloading curves have a reduced slope, which yields a significant reduction of the displacement with a small force excursion. Besides, algebraic and transcendental models have numerous advantages: the scholar does not need to solve differential equations. The drawback is the need to define continuity conditions between the selected algebraic or transcendental functions. In the considered structural systems, the transition between the loading and unloading curve is steep: there is almost a drop in the force value, see Figure 2. This nonsmooth transition could be obtained without continuity conditions or additional functions. The lack of continuity conditions in the mathematical formulation likely expresses the contact reduction between timber and connector from loading to unloading. The next section presents the formulation of an arctangent-based transcendental hysteresis model without continuity conditions.
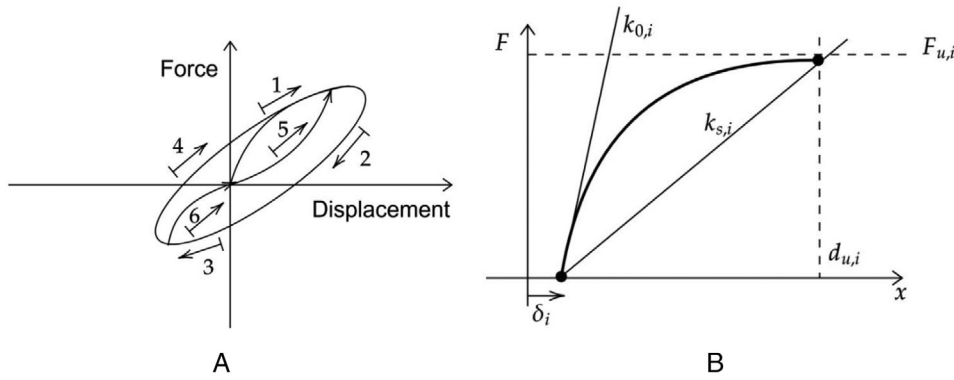
FIGURE 3 (A) Partition of a hysteresis cycle into six parts, identified by the sign of the displacement and velocity, and the occurring of pinching. (B) Mechanical parameters defining the features of a part of the cycle

3.1 | Model formulation

The authors point at reproducing a class of hysteresis phenomena identified by the following properties, using the arctangent function: pinching, significant stiffness reduction in the unloading phases, asymmetry of the hysteresis, strength degradation, and stiffness degradation. A hysteresis model based on the arctangent function may have the following piecewise definition:

$$
\begin{array}{llll}
1 & a_1 \arctan(b_1 x - |c_1|) & \text{if} & \{\dot{x} > 0,\ x > 0,\ |x| > q \max(|x(t)|) \forall t \in [0, t)\} \\
2 & a_2 \arctan(b_2 x - |c_2|) & \text{if} & \{\dot{x} < 0,\ x > 0\} \\
3 & a_3 \arctan(b_3 x + |c_3|) & \text{if} & \{\dot{x} < 0,\ x < 0\} \\
4 & a_4 \arctan(b_4 x - |c_4|) & \text{if} & \{\dot{x} > 0,\ x > 0,\ |x| < q \max(|x(t)|) \forall t \in [0, t)\} \\
5 & a_5 \arctan(b_5 x + |c_5|) & \text{if} & \{\dot{x} > 0,\ x < 0,\ |x| \leq q \max(|x(t)|) \forall t \in [0, t)\} \\
6 & a_6 \arctan(b_6 x + |c_6|) & \text{if} & \{\dot{x} > 0,\ x < 0,\ |x| \leq q \max(|x(t)|) \forall t \in [0, t)\}
\end{array}
\tag{6}
$$

where the six conditional statements identify the transition between the different parts of the hysteresis. A set of three parameters define the arctangent function in each section of the loop: a_i characterize the amplitude of the force, b_i the x axis resolution, and c_i the residual displacement. The subscript i varies between 1 and 6. The three parameters originate from the shape features of the associated section of the cycle. To enhance the clarity of the presentation, Figure 3(B) depicts the generic function in the first quadrant of the Cartesian plane. The main features of the i-th function are: the tangent stiffness ($k_{0,i}$), the secant stiffness ($k_{s,i}$), the yielding force ($F_{u,i}$), the displacement corresponding to the yielding force ($d_{u,i}$), and the residual displacement δ_i.

The definition of the parameters are: $a_i = \frac{2 F_{u,i}}{\pi}$, $b_i = \frac{k_0}{a_i}$, $c_i = |\delta_i|$. Exactly, a_i descends by equaling the horizontal asymptote to the maximum force, b_i by equaling the first derivative to the initial stiffness, while c_i has a direct correspondence with δ_i.

Additionally, the strength and stiffness degradation can descend from the use of an exponential function, like in Refs. [13, 17]. The exponential function expresses the force and stiffness degradation as a function of the dissipated hysteretic energy (ϵ). The energy-dependent definition of a_i and b_i is: $a_i(\epsilon) = e^{(-\xi_{a_i}\epsilon)} \frac{2 F_{u,i}}{\pi}$, $b_i(\epsilon) = e^{(-\xi_{b_i}\epsilon)} \frac{k_0}{a_i}$, where ξ_{a_i} and ξ_{b_i} are properly calibrated to the degradation of the strength and stiffness, respectively. The a_i, b_i, and c_i parameters descend directly from the experimental curve. Empirical hysteresis models, like the current one, always imitate experimental data. Therefore, the definition of the tangent stiffness, yielding force and yielding displacement from the experimental curve delivers the values of the parameters without the compelling need for the optimization algorithm. The authors cannot give the expected ranges of the parameters, since they are a function of the possible values of the tangent stiffness, yielding force and yielding displacement, which depend on the experimental curve. Conversely, the parameters of the exponential shape function, used to mirror the degrading behavior, may derive from a classical least-squares optimization[37] on the backbone curves, as carried out in the presented case studies. The most notable observation about this model is the ignoring of the continuity conditions. The crucial drawback of an algebraic or transcendental model, compared to a differential one, is the need to define continuity conditions between the loading and unloading curves. In this model, the absence of the
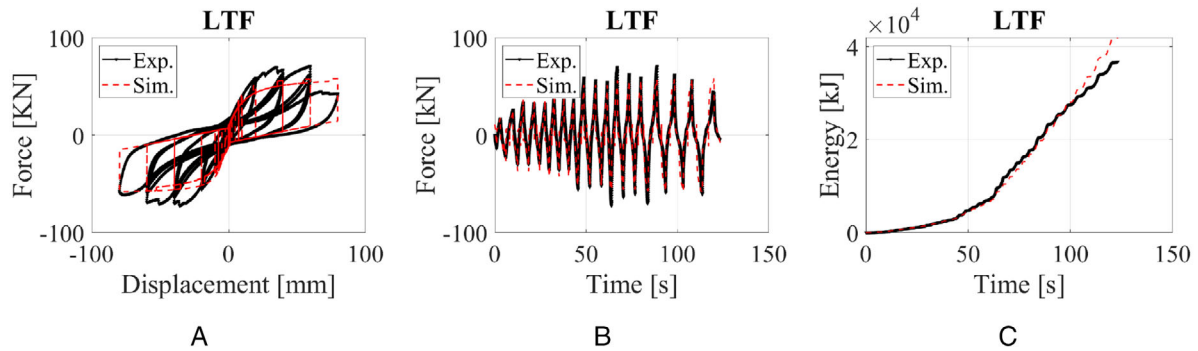
FIGURE 4   Comparison between the experimental cyclic response of an LTF shear wall and the stationary model; Exp. stands for experimental data, while Sim. for simulated data

continuity conditions descends from the observation of experimental data, see Figure 2. There is an almost vertical drop in force at the beginning of the unloading phase. The following sections will prove that the neglection of the continuity conditions between the loading and unloading curves may not cause a sensible error for engineering purposes. Conventional piecewise hysteresis models are continuous: each branch ends where the other begins, see the CUREE model.[27] Precisely, the coordinates of the ending point coincide with the coordinates of the beginning point. The suggested model is different and does not have continuity conditions in the unloading branches. In some structural systems, as occurs in timber connections, the unloading curve is significantly steep at the very beginning of the unloading phase, then the stiffness reduces, and it is minimal. This phenomenon descends from a shred of clear physical evidence: in timber joints, the steel connector loses contact with timber during the unloading phases causing the force to reduce drastically. The modeling of a nonlinear branch featured by a very high stiffness in the first instants of the unloading and an almost flat branch when the displacement reduces could be the source of several instability issues, as explained in the previous section. Therefore, the authors proposed an unloading branch characterized by a force discontinuity. The loading branch does end with the same displacement, which characterizes the unloading one. However, the loading curve's ultimate force value does not coincide with the initial force of the unloading: the unloading curve manifests a blunt force drop, which mirrors the physical loss of discontinuity between the steel connector and the adjacent timber.

4 | APPLICATION OF THE PROPOSED MODEL TO EXPERIMENTAL DATA

The paper presents an application of the model, named hereafter "Atan" model, to the experimental cyclic responses of LTF and CLT shear walls, and a steel angle bracket. The reader can find enough details of the experimental setup of CLT and LTF in Grossi et al.[36] The three experimental cyclic responses manifest a distinct progression of the strength and stiffness degradation: the authors examine the model capability in matching more complex hysteresis responses.

4.1 | Application to LTF shear walls

The experimental cyclic response, reported in Figure 2(A), manifests a smooth strength and stiffness degradation. Therefore, the exponential function is adequate to simulate such evolution. A stationary model, like the one in Figure 4, can be a compromise solution in the perspective of a direct simulation. In this paper, the term *stationary* identifies the independence of the model parameters on degradation phenomena or evolutionary behaviors. The model seizes the cyclic response, although it does not follow the exact curvature of the experimental data, due to the limits in using the arctangent function. Accurately, the loading curve follows the backbone curves, but it does not agree with the pinched paths, which have curvature opposite to the backbones and the arctangent function. Conversely, the unloading paths are adherent to the experimental data and, after the initial force drop, they exhibit the same slope. The observation of the plots reveals that the stationary model exhibits poor agreement, compared to other existing formulations,[24,38,39] due to the lack of degradation-dependent terms. Figure 4 shows that the crude nonstationary model should include degradation-dependent terms to achieve a good correspondence between the experimental and simulated data. The performance of

TABLE 1 Parameters of the hysteresis models depicted in Figures 4 and 5, labeled as stationary and degradation dependent, respectively

LTF		
Parameters	**Stationary**	**Degradation dependent**
$a_{i=\{1-6\}}$	38.217	44.586
$b_{1,4}$	0.236	0.202
$b_{2,3}$	0.008	0.022
$b_{5,6}$	0.131	0.112
$c_{i=\{2-3\}}$	0.300	0.300
$c_{i=\{1,4-6\}}$	0.200	0.200
$\xi_{a,b}$	0.000	8.000E-05

TABLE 2 The ultimate value of the simulated ($F_{u,s}$) and experimental forces ($F_{u,e}$), root mean square error (rmse), maximum error (me). and the relative maximum error to F_u (rme) corresponding to the models in Figures 4 and 5. The error is the difference between the experimental and simulated force vectors

LTF		
Error	**Stationary**	**Degradation-dependent**
$F_{u,s}$ (kN)	58.06	65.74
$F_{u,e}$ (kN)	71.00	71.00
rmse (kN)	22.11	11.61
me (kN)	12.94	5.26
rme (%)	18.22	7.40

the LTF panel is not stationary, but it exhibits a manifest dependence on stiffness and strength degradation: the resistance reduces, the stiffness diminishes, and it is minimal at the end of the cycle. Therefore, the stationary model is an in-between step toward a more advanced empirical hysteresis model discussed in the following paragraphs. Tables 1 and 2 present the values of the parameters and the corresponding error with the experimental data. The maximum error is notable due to the use of a stationary model: the strength reduces, but the model remains stationary.

The adoption of a strength and stiffness degradation function, like the exponential, improves the similarity between the hysteresis model and the experimental data significantly. Figure 5 depicts the results of a simulation obtained by using the parameters in Table 1. Even though the curvatures of the simulated and experimental data do not exhibit an exact matching, the comparison yields promising outcomes. The model follows the evolution of the degradation phenomena and grasps the peak force values attained by the LTF shear wall.
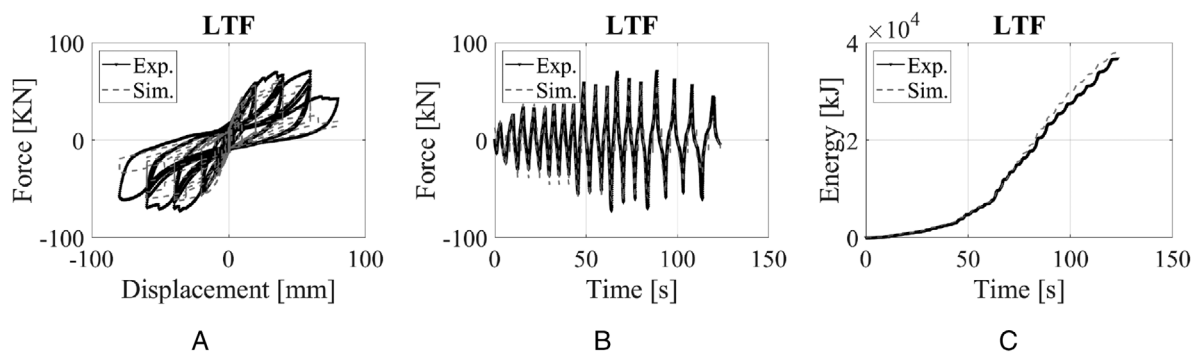
FIGURE 5 Comparison between the experimental cyclic response of an LTF shear wall and the degradation-dependent model; Exp. stands for experimental data, while Sim. for simulated data
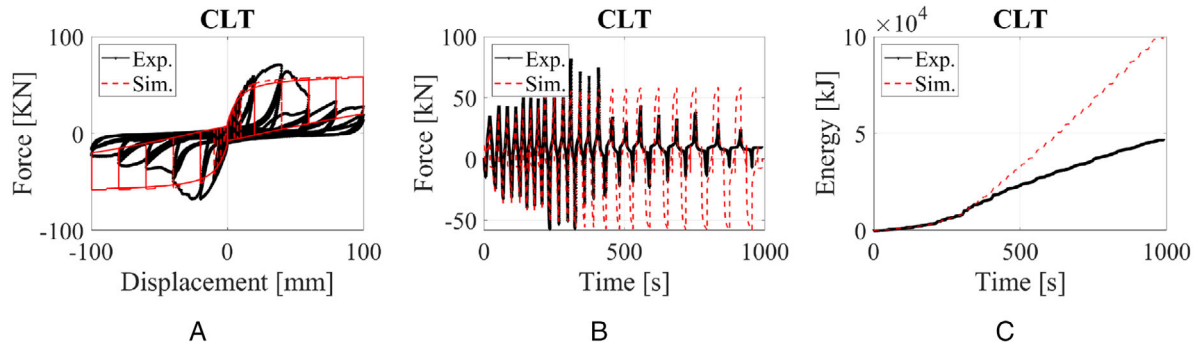
FIGURE 6 Comparison between the experimental cyclic response of a CLT shear wall and the stationary model; Exp. stands for experimental data, while Sim. for simulated data
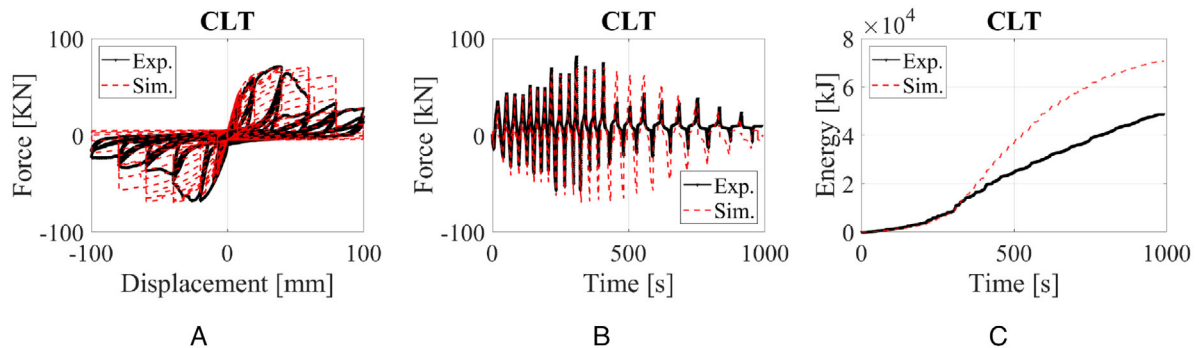

FIGURE 7 Comparison between the experimental cyclic response of a CLT shear wall and the degradation-dependent model; Exp. stands for experimental data, while Sim. for simulated data

4.2 | Application to CLT shear walls

The CLT shear walls exhibit a different cyclic response, characterized by an abrupt decrement in strength and stiffness to the failure of the hold-downs. The exponential decrement cannot replicate the sudden decrement of the force and the stiffness. The authors compared the experimental response of the CLT shear model to three models. The first is a stationary model characterized by constant values of the parameters. The second model has degradation-dependent parameters based on the use of an exponential function. The third model seeks an *ad hoc* piecewise function to reproduce the step-like decrement. Figure 6 presents the comparison with the stationary model in terms of hysteresis curve, force–time function, and energy–time function. The model hugely overestimates the force and energy values. Figure 7 displays the proposed model shaped by the exponential decrement function. The results improve, but the analytical model still exceeds the force and the dissipated energy. Figure 7(B) shows the force drop and the need in using an appropriate shape function. Still, the matching in Figures 6 and 7 is still inadequate, and a more elaborate model is needed. The authors adopted the following piecewise function to enhance the agreement between the analytical and experimental results. The drop corresponds to the dissipated energy associated with the strength fall.

$$\begin{cases} 1 & \text{if} \quad \epsilon < 1800 \text{ kJ} \\ 0.003 + e^{-0.001\epsilon} & \text{if} \quad \epsilon > 1800 \text{ kJ}. \end{cases} \tag{7}$$

Figure 8 shows the outcomes of the third model, obtained by using the step-like function in Equation (7). The correspondence increases, as confirmed by Table 4. Table 3 summarizes the parameters used to obtain the three hysteresis models illustrated in Figures 6, 7, and 8.

In conclusion, the adoption of a peculiar shape function can enhance the agreement between the experimental and simulated data significantly. The fact that the model crosses the origin of the axes and the lack of continuity conditions do not represent an hindrance to a satisfying matching.
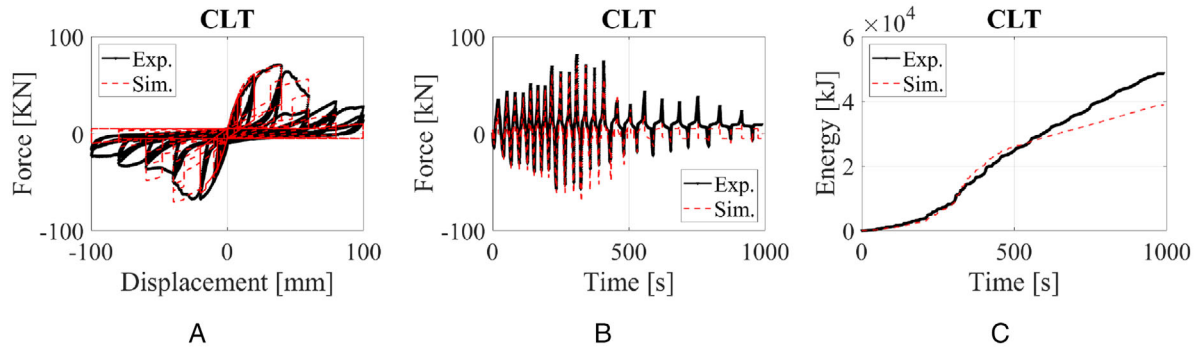
FIGURE 8 Comparison between the experimental cyclic response of a CLT shear wall and the degradation-dependent proposed model using a piecewise function for degradation; Exp. stands for experimental data, while Sim. for simulated data

TABLE 3 Parameters of the hysteresis models depicted in Figures 6, 7, and 8, labeled as stationary and degradation-dependent and degradation-dependent with exponential step, respectively

CLT			
Parameters	**Stationary**	**Degradation-dependent exp**	**Degradation-dependent exp step**
$a_{i=\{1-6\}}$	39.220	50.950	50.950
$b_{1,4}$	0.236	0.137	0.137
$b_{2,3}$	0.008	0.0196	0.0196
$b_{5,6}$	0.131	0.098	0.098
$c_{i=\{2-3\}}$	0.100	0.100	0.100
$c_{i=\{1,4-6\}}$	0.100	0.100	0.100
$\xi_{a,b}$	0.000	8.000E-05	Equation (7)

4.3 | Application to the pull-out of an angle bracket

The cyclic response of a steel angle bracket presents similar features to those manifested in the CLT and LTF shear walls. The performance of the Atan model is compared to the results of an FE simulation carried out in Abaqus. The investigation of a single connector, rather than an entire structural assembly, reduces the computational costs of a refined FE model in Figure 9 and encourages the implementation. Still, the analysis of a single connector entails notable computational efforts. Table 5 details the parameters of the Atan model used in the analysis. Figure 10 illustrates the cyclic response of the angle bracket in terms of hysteresis curve, force–time, and energy–time functions. Notwithstanding the notable simplifications, the Atan model with exponential decay exhibits a satisfying agreement with the experimental data. The angle bracket presents plasticization after a certain displacement level, yielding the arisen of opposing restoring forces.

TABLE 4 The ultimate value of the simulated ($F_{u,s}$) and experimental forces ($F_{u,e}$), root mean square error (rmse), maximum error (me), and the relative maximum error to F_u (rme) corresponding to the models in Figures 6, 7, and 8. The error is the difference between the experimental and simulated force vectors

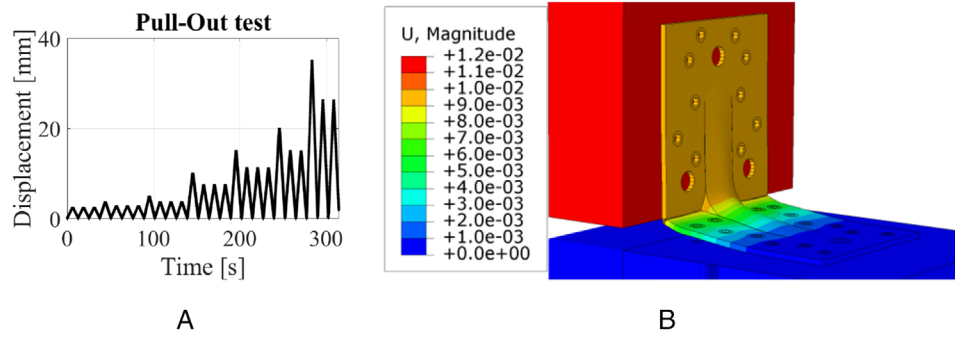| CLT			
Error	**Stationary**	**Degradation-dependent**	**Degradation-dependent exp step**
$F_{u,s}$ (kN)	58.36	70.31	75.61
$F_{u,e}$ (kN)	81.32	81.32	81.32
rmse (kN)	67.15	59.030	26.2
me (kN)	22.96	11.01	5.71
rme (%)	29.06	13.94	7.23

FIGURE 9 (A) Load protocol of the pull-out test, (B) FE model of the angle bracket

TABLE 5 Parameters of the hysteresis model in Figure 10; the ultimate value of the simulated ($F_{u,s}$) and experimental forces ($F_{u,e}$), root mean square error (rmse), maximum error (me), and the relative maximum error to F_u (rme) corresponding to the models in Figures 9 and 10. The error is the difference between the experimental and simulated force vectors

Angle bracket				
Parameters	Degradation-dependent exp	Error	Degradation-dependent exp	Abaqus
$a_{i=\{1,6\}}$	50.012	$F_{u,s}$ (kN)	41.39	40.46
$b_{1,4}$	0.376	$F_{u,e}$ (kN)	40.39	40.39
$b_{2,3}$	0.376	rmse (kN)	31.220	33.310
$b_{5,6}$	0.031	me (kN)	−1.00	−0.07
$c_{i=\{1,6\}}$	0.000	rme (%)	−2.48	−0.17
ξ_a	0.080			
ξ_b	0.010			

The negative forces are a small fraction of the positive ones. Both the Atan and the Abaqus model mirror the experimental data. However, the Atan model exhibits better accordance with them, as assessed in Table 5.

5 | VALIDATION WITH PSEUDO-DYNAMIC EXPERIMENTAL TESTS

This section deals with model validation. First, the authors calibrate the model on the experimental cyclic response of a given structural system. Then, the response of the already calibrated analytical model is compared to the experimental response of the same structural system excited by a different input. Precisely, the authors used the experimental cyclic response of plywood-coupled laminated-veneer lumber (LVL) wall panels, detailed in Ref. [40]. Iqbal et al. investigated the response of the same plywood-coupled LVL wall to pseudo-static and pseudo-dynamic loading and provides the details of the earthquake record used for the pseudo-dynamic test. Figure 11 shows the excellent agreement in terms of hysteresis
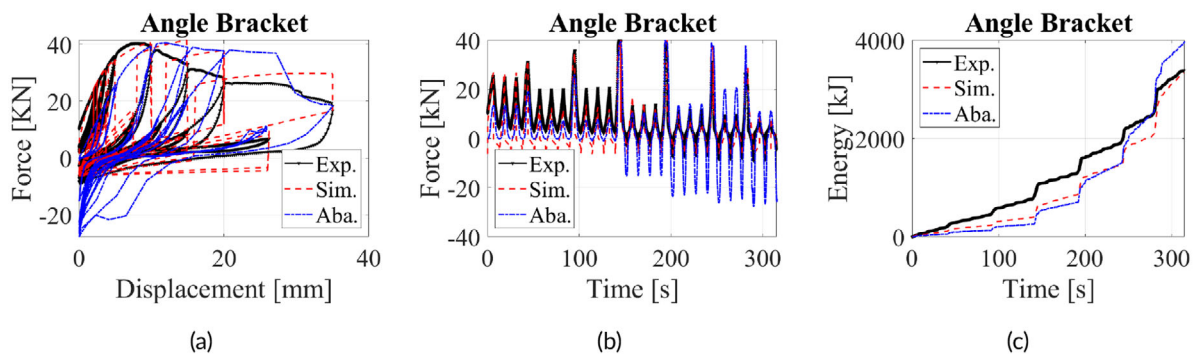

FIGURE 10 Experimental cyclic response on a plywood coupled LVL wall: (A) sketch and (B) front view of the panel
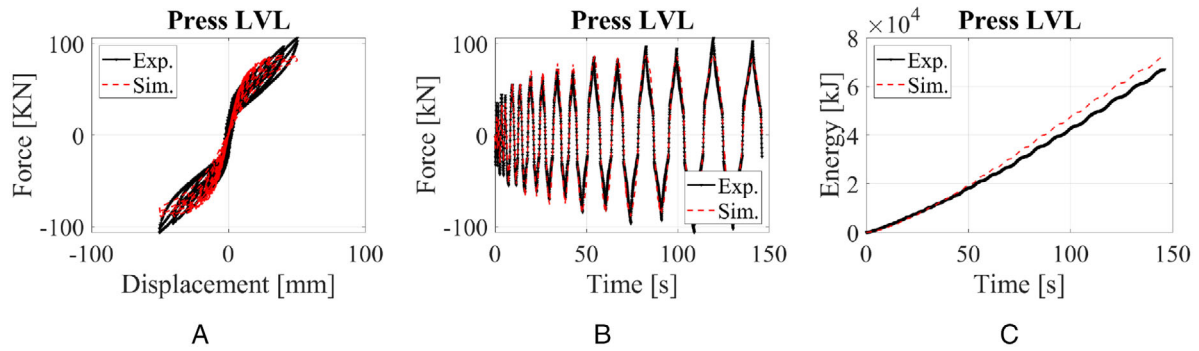
FIGURE 11 Comparison between the experimental cyclic response of a prestressed plywood-coupled LVL shear wall and the energy-dependent proposed model using a piecewise function for degradation; Exp. stands for experimental data, while Sim. for simulated data. Iqbal et al. provide full detail of the experimental setup in Ref. [40]

TABLE 6 Parameters of the hysteresis model in Figure 11

PRESS LVL	
Parameters	**Degradation-dependent exp**
$a_{i=\{1,6\}}$	70.060
$b_{1,4}$	0.114
$b_{2,3}$	0.099
$b_{5,6}$	0.099
$c_{i=\{1,6\}}$	0.000
$\xi_{a,b}$	7.000E-05

curve, force–time, and energy–time functions between the experimental tests and the proposed model with the parameters in Table 6. The comparison is satisfying, as notable from Table 7, possibly due to the reduced dissipative capacity of the structural system. Still, it manifests pinching and both strength and stiffness degradation as in most of the wood-based systems.

Figure 12 bestows the response of the real structural and the analytical model to pseudo-dynamic loading. The analytical model has been already calibrated, and the comparison between the two responses is a validation of the model: the scholar can theoretically use the model to extrapolate information using different inputs or, more generally, different structural configurations. Table 7 proves that the error associated with the pseudo-dynamic tests is not much higher than the one associated with the pseudo-static test. The model satisfactorily reproduces experimental data from cyclic tests, Figure 12. Consequently, experimental data could be considered adequately fitted for engineering purposes. In particular, the two responses are nearly coinciding in the central part of the graph, as evidenced in Figure 12(B).

TABLE 7 The ultimate value of the simulated ($F_{u,s}$) and experimental forces ($F_{u,e}$), root mean square error (rmse), maximum error (me), and relative maximum error to F_u (rmse) corresponding to the models in Figures 11 and 12. The error is the difference between the experimental and simulated force vectors

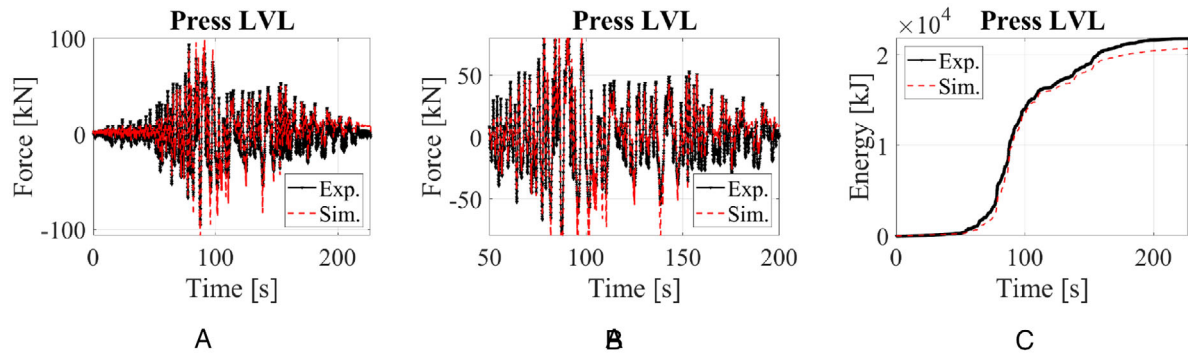|	PRESS LVL-atan model		PRESS LVL-eegbw model	
Error	**Pseudo-static**	**Pseudo-dynamic**	**Pseudo-static**	**Pseudo-dynamic**
$F_{u,s}$ (kN)	101.23	98.29	103.20	98.85
$F_{u,e}$ (kN)	106.50	96.01	106.50	96.01
rmse (kN)	13.85	23.31	13.85	33.31
me (kN)	5.27	−2.28	3.30	−2.84
rme (%)	4.95%	−2.37%	3.10%	−2.96%

FIGURE 12 Comparison between the response of a prestressed plywood-coupled LVL shear wall and the degradation-dependent proposed model under pseudo-dynamic tests; Exp. stands for experimental data, while Sim. for simulated data
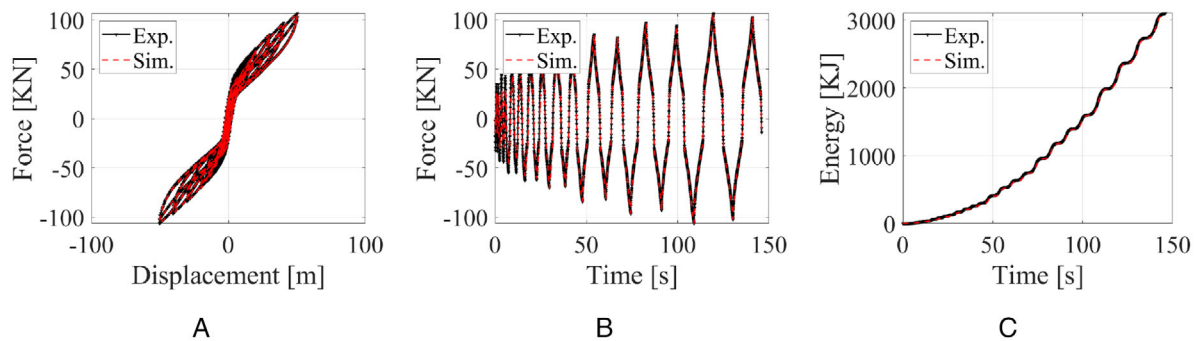

FIGURE 13 Comparison between the cyclic response of a prestressed plywood-coupled LVL shear wall and the extended energy-dependent generalized Bouc-Wen model under pseudo-static tests; Exp. stands for experimental data, while Sim. for simulated data

6 | COMPARISON WITH THE EXTENSION OF THE GENERALIZED BOUC-WEN MODEL: THE ISSUE OF NUMERICAL STABILITY

The authors would enrich the presentation by comparing the performance of a Bouc-Wen class model, the eegbw model[13] to the Atan model introduced in this paper. The Bouc-Wen class models are the most used differential models in structural dynamics. Accordingly, the authors compare the performance of the Atan model to a specific Bouc-Wen class model, the eegbw model, formulated for the simulation of the behavior of timber connections. The eegbw model can reproduce asymmetry, pinching, and degradation-dependent phenomena, compared to the enhancement of the Bouc-Wen model by Foliente,[17] which cannot reproduce asymmetrical responses. The versatility of the eegbw model in mirroring complex hysteretic behaviors supported its use for comparison purposes. The eegbw parameters associated with the optimum accordance with the experimental data are: $k_0 = 7000, \alpha = 0.12, \beta_1 = 1.66 + 0.002\epsilon, \beta_2 = -1.63 - 0.0003\epsilon, \beta_3 = 2.07 + 0.0003\epsilon, \beta_4 = -0.012 - 0.0004\epsilon, \beta_5 = 0.18 + 0.0001\epsilon, \beta_6 = -0.19 + 0.0002\epsilon, \beta_7 = 0, \beta_8 = 0, q = 0.9$. The calibration of the eegbw parameters is shown in Ref. [13]. The Bouc-Wen class models are described by a first-order ODE:

$$\dot{z} = \dot{x}[A - |z|^n \psi(z, \dot{x}, x)], \qquad (8)$$

where z is the inelastic variable, x the displacement, A and n constants, $\psi(z, \dot{x}, x)$ a shape function. The definition of the adopted shape function is detailed in Ref. [13]. The total resisting force f is:

$$f(x, \dot{x}, z) = \alpha k_0 x + (1 - \alpha)k_0 z, \qquad (9)$$

where α is the plasticity ratio and k_0 the initial stiffness. The eegbw model exhibits a notable performance, as evidenced by Figure 13. The model nearly seizes each section of the hysteresis curve, see Table 7. Additionally, Figure 14 and Table 4
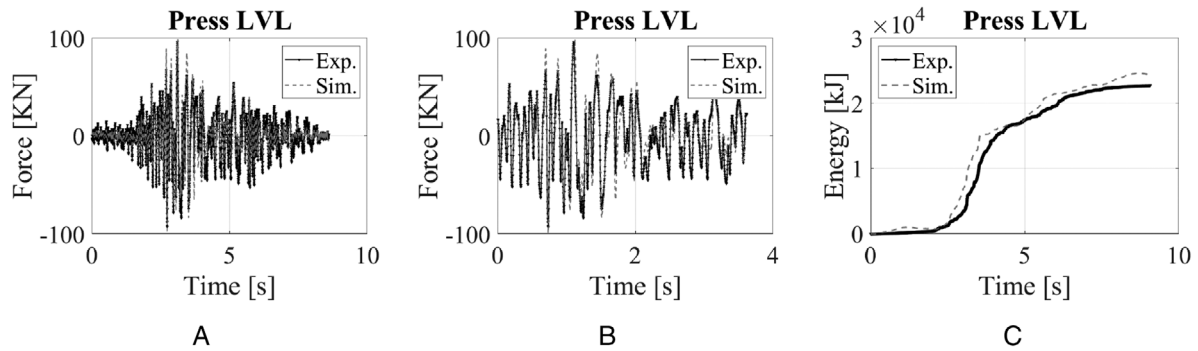
FIGURE 14 Comparison between the response of a prestressed plywood-coupled LVL shear wall and the extended energy-dependent generalized Bouc-Wen model under pseudo-dynamic tests; Exp. stands for experimental data, while Sim. for simulated data
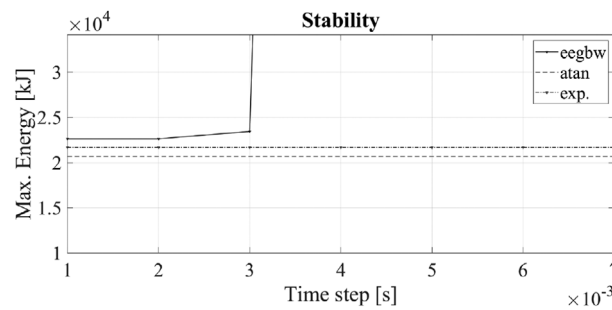

FIGURE 15 Stability of the eegbw model to the integration time step, obtained by varying the amplitude of the time step in the pseudo-static simulation

validate the eegbw model using the experimental response to pseudo-dynamic excitation and confirm that there is a substantial agreement between the eegbw model and the experimental response.

Though, differently from algebraic or transcendental models, the restoring force in Bouc-Wen class models originates from the solution of a first-order differential equation. In current situations, the solution descends from numerical integration. Several algorithms can ensure proper convergence of the solution; however, the endeavor for convergence may entail additional computational costs. In some instances, the difficulty in convergence may raise the computational costs to unreasonable durations of the simulations.

The authors attempted to illustrate the role of convergence in Figure 15 by varying the sampling interval in the eegbw model. The occurrence of instability manifests as an abrupt growth of the force or displacement values: the forcing term can push the model to out-of-range values of the hysteresis curve. The authors chose the approximate dissipated energy as a synthetic parameter to reveal the occurrence of instability. If the approximate dissipated energy blows up, the model attained out-of-range values of the displacement or force values. Accurately, instability issues are sensitive to the value of the integration step: higher integration steps lead to larger displacement steps, which can lead the pinched paths to attain out-of-range values. Therefore, the authors varied the integration step in a given interval to observe the possible occurrence of nonconvergence. The sampling interval associated with the pseudo-dynamic loading is 0.001 s. It tested the stability of the integration, without any convergence algorithm, in the range 0.001–0.007 s. Figure 15 reports the maximum value of the approximate dissipated energy, named Max. Energy, as a function of the integration step, is named Time step. Figure 15 proves that the Bouc-Wen model begins manifesting stability issues since a 0.003 s time-step, where the dissipated energy boosts. Conversely, the dissipated energy of the Atan model is stable, since the force value is algebraic and so defined at each time step without the need of any antecedent value. The maximum dissipated energy of the experimental test is set stationary to the velocity of the integration by disregarding possible viscous effects which may raise its value. These rudimentary passages do not demonstrate the instability of the eegbw model, since dynamic simulations should always be driven by suitable convergence algorithms to obtain consistent results. However, the more the model is prone to instabilities, the more the convergence algorithm must lessen the integration step with possibly inconvenient raise of the computation time. On the contrary, algebraic and transcendental models may have several advantages. Primarily, they
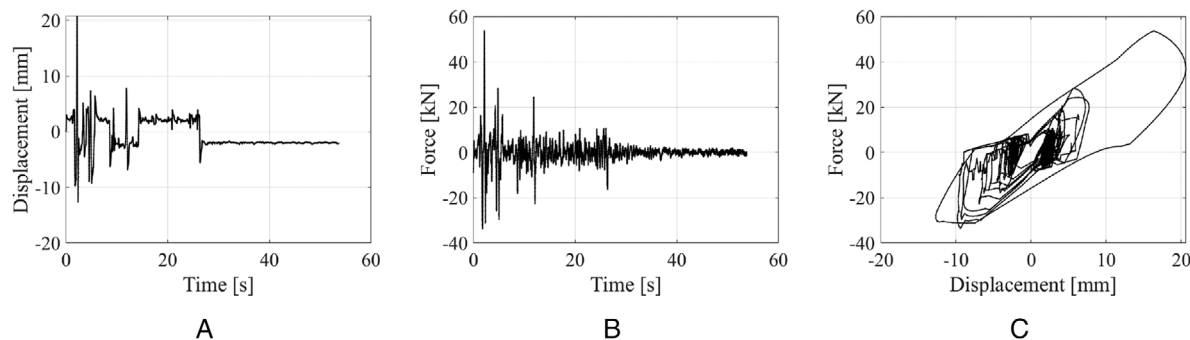
FIGURE 16 Seismic response to the El Centro earthquake of a simplified structural archetype defined in terms of the Atan model

do not require the solution of a differential equation. Additionally, if the model is upper bounded, the excitation would never cause abrupt boosts if the time step is too much loose. At this stage, the authors wonder if using an algebraic or transcendental model with a bit higher discrepancy with the experiments may be more beneficial than using a differential hysteresis model. The differential hysteresis model may sharply seize the experimental response but could be critically prone to numerical instabilities, which may compromise the advantage in using empirical formulations. Several scholars favor empirical hysteresis models, that is, models without any mechanical establishing that blindly match the experimental data, to carry out faster analyses. However, if the hysteresis model is vulnerable to instabilities, the computational costs could make impractical their use in structural calculations. Therefore, their intrinsic vulnerability may erode their computational advantages.

6.1 | Nonlinear dynamic analysis

The preceding sections exposed the performance of the Atan model under a given displacement history, quasi-static, or pseudo-dynamic. This subsection bestows a further demonstration of the Atan model performance in a full dynamic analysis. The authors solved the nonlinear ODE of a SDOF oscillator, where the Atan model describes the resisting inelastic force. In contrast with the previous sections, the displacement is unknown and must descend from the numerical integration of the ODE. Precisely, the authors used the explicit fourth-order Runge-Kutta method for the temporal discretization of the approximate solution of the ODE. It is considered an inelastic SDOF oscillator, representative of an LTF shear wall in Figure 5, which bears a 1000 kg mass. The ODE representative of the nonlinear dynamic response of an LTF shear wall under earthquake excitation is:

$$m\ddot{x} + f_s = -m\ddot{x}_g, \tag{10}$$

where m is the mass, x the displacement, $\ddot{x}$ the double derivative of x with respect to time, f_s the resisting inelastic force, and $\ddot{x}_g$ the ground acceleration. In this example, the authors used a recording of the El Centro earthquake. Figure 16 illustrates the displacement–time, velocity–time, force–time, and force–displacement curves. The results are comforting since the model exhibits a stable performance under earthquake excitation. Besides, the displacement–time plot manifests the occurrence of a residual drift, which represents precious information in the postearthquake assessments. The hysteresis curve manifests all features of timber connections, pinching, and degradation phenomena. Regrettably, these results do not have the experimental counterpart to provide a full validation.[41] Although, this section serves as a further demonstration of the model performance under earthquake excitation.

7 | CONCLUSIONS

This paper presents the "Atan" model, a transcendental hysteresis model possibly useful to reproduce the hysteresis response of wooden structural systems characterized by notable pinching and degradation effects. The primary aspects addressed by this paper are:

- The so-labeled Atan model originates from the piecewise definition of the arctangent function shaped by constant or time-varying parameters, depending on the degradation phenomena to follow. The main features of the hysteresis loop, like the ultimate force and the initial stiffness, yield a direct definition of the parameters of the arctangent functions.

- The authors adopted the proposed model to match the experimental cyclic response of LTF, CLT shear walls, and an angle bracket, characterized by distinct stiffness and strength decay. The LTF and the angle bracket required the adoption of an exponential function to seize the observed lowering in strength and stiffness. Conversely, the CLT required a step-like shape function to reproduce the abrupt fall in strength and stiffness due to the sudden failure of the hold-downs.

- The experimental cyclic response to pseudo-static and pseudo-dynamic excitation of a plywood-coupled LVL wall panel validated the proposed Atan model. The authors compared the pseudo-dynamic response of the Atan model, calibrated on the pseudo-static cyclic data, with the experimental cyclic response to the same pseudo-dynamic excitation. The comparison yields satisfactory results and endorses the usefulness of the proposed model.

- In the last section, the authors address the importance of dealing with numerically stable and upper bounded hysteresis models to have consistent results without a significant rise in computational time. A Bouc-Wen class model is used to explain these concepts and remark on the advantages of using algebraic or transcendental models, like the one presented in this paper.

- Future research efforts will focus on implementing the Atan model as a new user-defined element in Abaqus to simulate the nonlinear dynamic response of more complicated structural arrangement. The computational and stability advantages of the Atan model and the Abaqus capability in assembling the stiffness matrix may support the development of reliable and efficient nonlinear springs for the simulation of nonlinear structural responses.

ORCID

Angelo Aloisio https://orcid.org/0000-0002-6190-0139

REFERENCES

1. Aloisio A, Pasca D, Tomasi R, Fragiacomo M. Dynamic identification and model updating of an eight-storey CLT building. *Eng Struct*. 2020;213: 110593.
2. Aloisio A, Alaggio R, Fragiacomo M. Fragility functions and behavior factors estimation of multi-story cross-laminated timber structures characterized by an energy-dependent hysteretic model. *Earthquake Spectra*. 2020:8755293020936696. https://doi.org/10.1177/8755293020936696
3. Aloisio A, Alaggio R, Fragiacomo M. Equivalent Viscous Damping of Cross-Laminated Timber Structural Archetypes. *J Struct Eng*. 2021;147(4):04021012
4. Aloisio A, Fragiacomo M. Reliability-based overstrength factors of cross-laminated timber shear walls for seismic design. *Eng Struct*. 2021;228:111547.
5. Blandon CA, Priestley M. Equivalent viscous damping equations for direct displacement based design. *J Earthq Eng*. 2005;9(sup2):257-278.
6. Kivell B, Moss P, Carr A. Hysteretic modelling of moment-resisting nailed timber joints. *Earthq Eng*. 1981;14(4):233-245.
7. Dowrick D. Hysteresis loops for timber structures. *Bull New Zealand Soc Earthq Eng*. 1986;19(2):143-152.
8. He M, Lam F, Foschi RO. Modeling three-dimensional timber light-frame buildings. *J Struct Eng*. 2001;127(8):901-913.
9. Yang JQ, Smith ST, Wang Z, Feng P, Sirach N. Modelling of hysteresis behaviour of moment-resisting timber joints strengthened with FRP composites. *Int J Mech Sci*. 2020;179:105593.
10. Vogrinec K, Premrov M, Šilih EK. Simplified modelling of timber-framed walls under lateral loads. *Eng Struct*. 2016;111:275-284.
11. Jayamon J, Charney F, Flores F, Line P. Influence of wall load-displacement shape on seismic performance of wood-frame shear wall structures. In: World Conference on Timber Engineering, Vienna, Austria 2016.
12. Anil Ö, Togay A, Işleyen ÜK, Döngel N, Söğütlü C. Effect of timber type and nail spacing on the hysteretic behavior of timber-framed shear walls with openings. *Int J Civ Eng*. 2018;16(6):629-646.
13. Aloisio A, Alaggio R, Köhler J, Fragiacomo M. Extension of generalized Bouc-Wen hysteresis modeling of wood joints and structural systems. *J Eng Mech*. 2020;146(3):04020001. https://doi.org/10.1061/(ASCE)EM.1943-7889.0001722
14. Visintin A. Genesis of hysteresis. In: *Differential models of hysteresis*. Applied Mathematical Sciences Berlin, Heidelberg: Springer. 1994:12-31.
15. Bouc R. Solution periodique de lequation de la ferroresonance avec hysteresis. *Comptes Rendus Hebdomadaires Des Seances De L Academie Des Sciences Serie A*. 1966;263(15):497.

16. Baber TT, Wen YK. Random vibration hysteretic, degrading systems. *J Eng Mech Div*. 1981;107(6):1069-1087.

17. Foliente GC. Hysteresis modeling of wood joints and structural systems. *J Struct Eng*. 1995;121(6):1013-1022.

18. Krasnosel'skii MA, Pokrovskii AV. *Systems with Hysteresis*. Berlin, Heidelberg: Springer Science & Business Media; 2012.

19. Mayergoyz I. The classical Preisach model of hysteresis. In: *Mathematical Models of Hysteresis*. Berlin, Heidelberg: Springer; 1991: 1-63.

20. Ismail M, Ikhouane F, Rodellar J. The hysteresis Bouc-Wen model, a survey. *Arch Comput Methods Eng*. 2009;16(2):161-188.

21. Amor YO, Féliachi M, Mohellebi H. A new convergence procedure for the finite element computing associated to Preisach hysteresis model. *IEEE Trans Magn*. 2000;36(4):1242-1245.

22. Laudani A, Fulginei FR, Salvini A. Bouc–Wen hysteresis model identification by the metric-topological evolutionary optimization. *IEEE Trans Magn*. 2014;50(2):621-624.

23. Polensek A, Laursen HI. *Seismic Behavior of Bending Components and Intercomponent Connections of Light Frame Wood Buildings*. Corvallis, OR: Oregon State University; 1984.

24. Rinaldin G, Amadio C, Fragiacomo M. A component approach for the hysteretic behaviour of connections in cross-laminated wooden structures. *Earthq Eng Struct Dyn*. 2013;42(13):2023-2042.

25. Di Gangi G, Demartino C, Quaranta G, Monti G. Dissipation in sheathing-to-framing connections of light-frame timber shear walls under seismic loads. *Eng Struct*. 2020;208: 110246.

26. Folz B, Filiatrault A. Seismic analysis of woodframe structures. I: Model formulation. *J Struct Eng*. 2004;130(9):1353-1360.

27. Pang W, Rosowsky D, Pei S, Lindt V. dJ. Evolutionary parameter hysteretic model for wood shear walls. *J Struct Eng*. 2007;133(8):1118-1129.

28. Judd JP, Fonseca FS. Analytical model for sheathing-to-framing connections in wood shear walls and diaphragms. *J Struct Eng*. 2005;131(2):345-352.

29. Blasetti A, Hoffman R, Dinehart D. Simplified hysteretic finite-element model for wood and viscoelastic polymer connections for the dynamic analysis of shear walls. *J Struct Eng*. 2008;134(1):77-86.

30. Dolan JD. *The Dynamic Response of Timber Shear Walls*. [PhD thesis]. University of British Columbia; 1989.

31. Xu J, Dolan JD. Development of a wood-frame shear wall model in ABAQUS. *J Struct Eng*. 2009;135(8):977-984.

32. Baber TT, Noori MN. Random vibration of degrading, pinching systems. *J Eng Mech*. 1985;111(8):1010-1026.

33. Wen YK. Method for random vibration of hysteretic systems. *J Eng Mech Div*. 1976;102(2):249-263.

34. Noël JP, Kerschen G. Nonlinear system identification in structural dynamics: 10 more years of progress. *Mech Syst Signal Process*. 2017;83:2-35.

35. Carboni B, Lacarbonara W, Brewick PT, Masri SF. Dynamical response identification of a class of nonlinear hysteretic systems. *J Intell Mater Syst Struct*. 2018;29(13):2795-2810.

36. Grossi P, Sartori T, Tomasi R. Tests on timber frame walls under in-plane forces: part 2. *Proc Inst Civil Eng-Struct Build*. 2015;168(11):840-852.

37. Aloisio A, Alaggio R, Fragiacomo M. Dynamic identification of a masonry façade from seismic response data based on an elementary Ordinary Least Squares approach. *Engineering Structures*. 2019;197:109415. https://doi.org/10.1016/j.engstruct.2019.109415.

38. Folz B, Filiatrault A. CASHEW-Version 1.0: A Computer Program for Cyclic Analysis of Wood Shear Walls. Richmond, California; 2000.

39. Dolan J, Foschi R. Structural analysis model for static loads on timber shear walls. *J Struct Eng*. 1991;117(3):851-861.

40. Iqbal A, Fragiacomo M, Pampanin S, Buchanan A. Seismic resilience of plywood-coupled LVL wall panels. *Eng Struct*. 2018;167:750-759.

41. Aloisio A, Antonacci E, Fragiacomo M, Alaggio R. The Recorded Seismic Response of the Santa Maria Di Collemaggio Basilica to Low-intensity Earthquakes. *International Journal of Architectural Heritage*. 2020;1–19. https://doi.org/10.1080/15583058.2020.1802533.